JOURNAL OF MATERIALS SCIENCE 16 (1981) 439–450

Kinking and tensile, compressive and interlaminar shear failure in carbon-fibre-reinforced plastic beams tested in flexure

T. V. PARRY, A. S. WRONSKI
School of Materials Science, University of Bradford, West Yorkshire, UK

The first stage of the failure process in pultruded, 60% volume fraction, type III carbon fibre–epoxide beam specimens with span-to-depth ratios of 5, 15 and 40 deformed in flexure at atmospheric pressure was the initiation of kinking by the "compression" roller. Kink growth during the non-linear part of the load–deflection curve was followed by kink propagation at peak load. Acoustic emission and load–unload tests to detect irrecoverable deflection supported direct microscopic observations of damage. Kink growth with decreasing load, increasing deflection and accompanying redistribution of stresses led to two types of failure, commonly referred to as "flexural" and "interlaminar". In the former, tensile failure was concurrently initiated to give the characteristic tensile and compressive zones on the failure surfaces. In the latter, the growing kink initiated interlaminar cracks in resin-rich zones as it propagated (with decreasing load) towards the convex surface. Kinking was associated with triaxial compressive stresses in the contact zone of the "compressive" roller or rollers (in the case of four-point bend specimens). When hydrostatic pressure was superposed on flexure, at pressures between 150 and 300 MN m^{-2} depending on the type of specimen, kinking was inhibited and eventually suppressed to give tensile failures, even in the so-called interlaminar shear strength type of specimen. When non-linear deflections were not large, the maximum principal tensile stress in the beams was close to the tensile strength of the carbon-fibre-reinforced plastic ($\sim$ 1.8 GN m^{-2}).

1. Introduction

Rectangular beam specimens are commonly used to measure, depending on the specimen span-to-depth ratio, the "flexural strength" and the "interlaminar shear strength" (ILSS) of unidirectionally aligned, continuous, carbon fibre–resin composites. "Tensile", "interlaminar shear" and "compressive" are the generally recognized mechanisms of failure; the tensile mode is postulated to result from fibre breaks and debonding [1] and the compressive mode is associated with fibre shear [2] and/or buckling [3], compression creases [4] or kinking [5–7]. Kinking during axial compression of unidirectional carbon-fibre-reinforced plastics (CFRP) has been described as the mechanism of transverse deformation whereby shear takes place initially parallel (or nearly so) to the principal stress (and therefore the fibre) axis [5]. It has been also observed in glass-reinforced plastic [6], timber [8], rocks [9] and even books or stacks of cards [10]. In composite and laminar structures, kinks form by the rotation of parallel lamellae away from the original position. During kink growth the kink bands develop diagonally across the sample and this, it is suggested, necessitates rotation and failure of the fibres by buckling [5].

The maximum loads recorded during testing

0022–2461/81/020439–12$03.20/0

of rectangular CFRP beam specimens tend to be used to evaluate the relevant strength [11], irrespective of the non-linearity of the load–deflection behaviour which frequently precedes the attainment of these loads. When observed in tensile tests, acoustic emission associated with this behaviour has been principally ascribed to accumulation of fibre damage [12] and resin cracking. Particularly in flexure, however, there seems to have been insufficient attention paid to the initiation, growth and propagation of the failure processes in unidirectionally-aligned CFRP and to the relationships of these stages with material and testing parameters. The unsatisfactory nature of the association of conventional strength parameters with failure mechanisms in CFRP can be illustrated by the following examples.

In a study of the properties of CFRP reinforced with steel wires (of similar elastic properties to the type III carbon fibres) near the tensile and/or compressive surfaces. Bradley and Harris [13] reported that the ILSS (measured on the *neutral* plane) was raised from the value characteristic for the composite if the steel wires were in the compressive surface or in both surfaces. Parry and Wronski [14] have observed an increase in the so-called ILSS of a given batch of CFRP from 75 to 88 $MN\,m^{-2}$ when the diameter of the loading rollers was simply raised from 2.0 to 6.3 mm. In presenting data on strengths of CFRP determined in tension, Hitchon *et al.* [15] noted clean breaks (at sample waist and not at sample waist), staggered irregular breaks, shear failure and mixed tensile–interlaminar shear failure, yet evaluated "fibre strength" in all cases. For the strategically reinforced CFRP of Bradley and Harris [13], flexural strengths were higher if the wires were positioned only in the compressive surface than if placed only in the tensile surface. Further, a consistent increase in flexural strength with wire content (of similar elastic modulus to the fibre and smaller yield strain than the fibre breaking strain) was then recorded. Finally, the theories of composite compressive strength generally associate its value with the shear modulus of the matrix. It is noteworthy that the compressive strength of a carbon-fibre–nickel composite [16], $\sim 0.9\,GN\,m^2$, is comparable to that of a carbon-fibre–epoxy composite, although the shear modulus of the nickel, $77\,GN\,m^2$, is nearly two orders of magnitude larger than that of the resin.

Consideration of the mechanisms of deformation and failure of CFRP in axial tension [17] and compression [5] and transverse compression [18] has been aided by data obtained in studies of these straining modes under complex loading. A major part of this investigation was the assessment of the effects of superposed hydrostatic pressure on the failure mechanisms and failure modes resulting from the bending of CFRP beams.

2. Theory: bending and concentrated loads

In elementary (Bernouilli–Euler) beam theory the effect of concentrated loads (rollers in our case) is neglected and the maximum tensile and compressive stresses in three-point bending are given by the formula [19]

$$\sigma = 3PL/2wt^2, \tag{1}$$

which is conventionally used to present data on composites; here P is the load, L is the span, w is the width and t is the depth of the beam. The maximum (interlaminar) shear stress (on this neutral plane), given by the same theory, is

$$\tau = 3P/4wt. \tag{2}$$

The effect of concentrated loads, particularly for beams with small span-to-depth ratios, is important, as has been clearly demonstrated by photoelastic techniques [20, 21]; their relevance to testing has been acknowledged primarily with respect to the determination of maximum tensile stress (modulus of rupture), σ_T, of brittle materials [22, 23], when the following formula was used [24, 25]:

$$\sigma_T = \frac{3PL}{2wt^2} - \frac{0.266P}{wt}. \tag{3}$$

In deriving this relation the effect of the compressive roller, assuming concentrated line loading, a distance t away, is considered. The procedure takes note of the similarity of the stress distribution in the vicinity of the loading line, evident from photoelastic studies, to that produced in a semi-infinite plate by a normal concentrated force. The procedure of superposition involves the replacement of radial compressive stresses acting on the sections corresponding to the rectangular beam faces by equal radial tensile stresses acting on the actual beam faces. Accordingly, the solution considers the superposition of the bending forces, the radial tensile forces and the concentrated force. The exact solution of von Karman and Seewald [24] yields an infinite compressive

correction factor for the through thickness stress, σ_y, and does not evaluate the longitudinal correction factor to the simple beam formula. At a distance $x \sim 0.04t$ along the beam, however, the maximum correction factor for σ_x is a tensile stress of $1.232\ P/wt$. An approximate solution, in which a continuously distributed load is applied to the bottom of the beam [25] gives the compressive bending stresses

$$\sigma_x(\mathrm{B}) = \frac{12P}{t^3 w}\left(\frac{L}{4} - \frac{t}{2\pi}\right)y + \frac{P}{\pi tw} + \frac{2P}{\pi tw}\left(\frac{4y^3}{t^3} - \frac{3y}{5t}\right) \tag{4}$$

and

$$\sigma_y(\mathrm{B}) = \frac{P}{\pi tw} + \frac{2P}{\pi tw}\left(\frac{3y}{2t} - \frac{2y^3}{t^3}\right), \tag{5}$$

where $-y$ is the distance from the neutral axis. Timoshenko and Goodier [25] superposed these stresses on the concentrated line stresses to obtain

$$\sigma_x(\mathrm{L}) = 0 \tag{6}$$

and

$$\sigma_y(\mathrm{L}) = \frac{2P}{\pi(\frac{1}{2}t + y)w}. \tag{7}$$

It seems to the authors, however, more appropriate to consider Hertzian stresses, which give a compressive correction factor $\sigma_x(\mathrm{H})$. Following Huber and Fuchs [26] and Poritsky [27], Childs [28] suggests, instead of $\sigma_x(\mathrm{L})$ and $\sigma_y(\mathrm{L})$, compressive stresses

$$\sigma_x(\mathrm{H}) = \frac{2Py_1}{\pi a^2 w}\left[\left(\frac{a^2+u}{u}\right)^{1/2}\left(2 - \frac{a^2 y_1^2}{u^2 + a^2 y_1^2}\right) - 2\right] \tag{8}$$

and

$$\sigma_y(\mathrm{H}) = \frac{2P}{\pi w}\frac{y_1^3}{u^2 + a^2 y_1^2}\left(\frac{a^2+u}{u}\right)^{1/2}, \tag{9}$$

where

$$u = \tfrac{1}{2}\{x^2 + y_1^2 - a^2 + [(x^2 + y_1^2 - a^2)^2 + 4a^2 y_1^2]^{1/2}\},$$

$$y_1 = c + y$$

and a is the half-width of the contact. The maximum values of $\sigma_x(\mathrm{H})$ and $\sigma_y(\mathrm{H})$ occur at the loading line $y_1 = 0$, when

$$\sigma_x(\mathrm{H}) = \sigma_y(\mathrm{H}) = 0.565\left(\frac{PE^1}{wR^1}\right)^{1/2}, \tag{10}$$

where

$$\frac{1}{E^1} = \frac{1}{E_r} + \frac{1}{E_b} \simeq \frac{1}{E_b}$$

and

$$\frac{1}{R^1} = \frac{1}{R_b} + \frac{1}{R_r} \simeq \frac{1}{R_r}.$$

E_r is the Young's modulus of the roller, approximately equal to $40E_b$, E_b being the transverse Young's modulus of the CFRP beam ($\sim 5\ \mathrm{GN\,m^{-2}}$) and R_b and R_r are the radii of curvature of the beam and roller, respectively.

The compressive stresses at the loading line are therefore suggested to be

$$\sigma_x = \frac{P}{wt}\left(\frac{3L}{2t} - 1.146\right) + 0.565\left(\frac{PE^1}{wR^1}\right)^{1/2} \tag{11}$$

and

$$\sigma_y = 0.565\left(\frac{PE^1}{wR^1}\right)^{1/2}. \tag{12}$$

3. Experimental procedure

3.1. Preparation of the specimens

The material for this investigation was obtained from Courtaulds Ltd in the form of pultruded sections, 2 mm thick and 10 mm wide. The pultrusions contained ~60% volume fraction of Grafil A-S (type III carbon-fibre) in epoxy resin. For the majority of tests the specimen thickness was 2 mm; for some it was 1.5–1.7 mm (the specimens being ground to the required thickness on a surface grinding machine using a coarse, open grit wheel). Specimen widths were ~10 mm and test spans were mainly 10, 25 or 80 mm to give span-to-depth ratios of 5, ~15 and 40.

3.2. Mechanical testing

The majority of the atmospheric pressure flexural tests were performed on a Hounsfield machine modified to incorporate a Baldwin–Lima–Hamilton (BLH) semiconductor load cell and a compression cage with a range of support spans. To monitor mid-span defelction a linear variable differential transformer (LVDT) was employed and this enabled the recording of load–deflection plots on an x–y recorder. Roller diameters were generally 6.35 mm and the cross-head speed was $1\ \mathrm{mm\ min^{-1}}$.

Some of the tests at atmospheric pressure and all the tests under superposed pressure were carried out on a Hedeby tension/compression tester fitted with a Coleraine pressure cell. Two three-point bending jigs [29] incorporating load cells were constructed to test specimens with spans up to 25 mm (Fig. 1). For longer spans the cylindrical yoke assembly previously used [30] was replaced by one of rectangular section through which the load cell and loading roller attachment were connected to the upper pull rod. The outher cylinder was replaced by a bar of the same length and diameter,

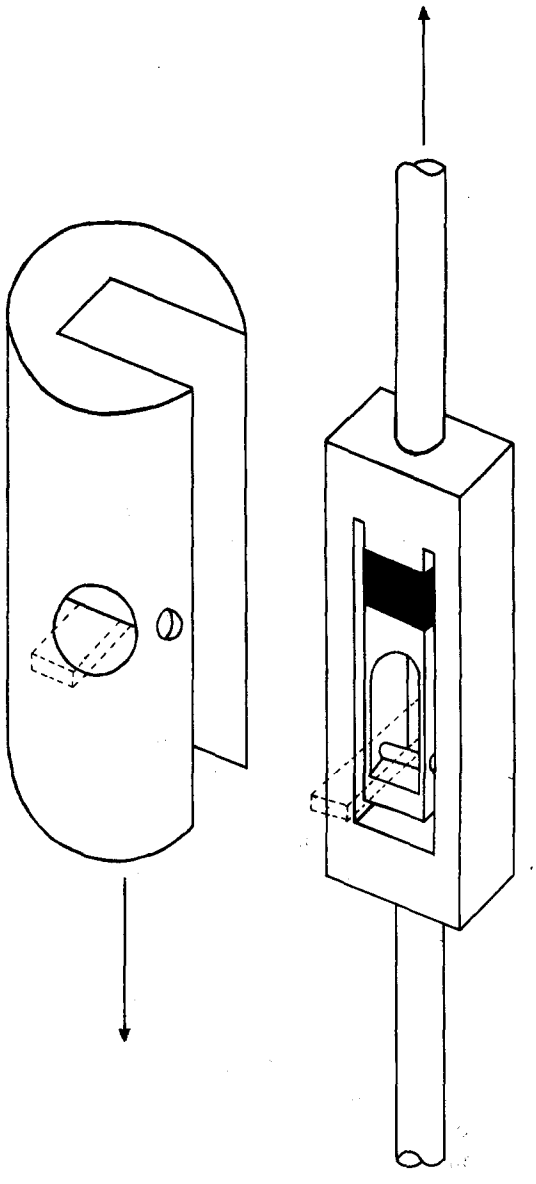

Figure 1 A sketch of the components of the pressure cell rig, which is assembled prior to insertion of a (25 mm span) specimen. The position of the specimen is indicated in relation to the loading rollers in both components.

but with a machined channel through which the yoke could slide. It contained the two supporting rollers and exposed a hole perpendicular to the channel through which the specimen was fitted. An important feature of this arrangement is that, unlike in previous work [30], bending occurs when the machine operates in the tensile mode, which reduces alignment problems.

By replacing the single loading roller by two, four-point bending testing was also carried out. The load was measured using the internal resistance load cell and monitored with the aid of the external semiconductor load cell, which registered the sum of applied load and frictional forces. Specimens with spans of 10 mm were tested in three-point bending using the first jig; three-point bend tests on spans of 25 mm and four-point bend tests on specimens with 8.25 mm inner–outer roller distance were made using the second assembly. Some tensile plate specimens, with thicknesses reduced from 2 mm to 1 mm at the centre, were tested on the Hedeby machine.

The deformation at atmospheric pressure of several specimens with span-to-depth ratios of 40 and 5 was monitored with an Acoustic Consultants acoustic emission counter. At ambient pressure 'load–unload' cycling was also performed with increasing load range and the onset of permanent deflection noted. Deformation of some beams was stopped prior to and beyond the peak load for microscopic examination. Several beams were polished through the width to observe details of the damage preceding complete beam failure. Failed specimens were examined on an ISI Super III scanning electron microscope.

4. Results

4.1. Flexural modulus

Six specimens with span-to-depth (2 mm) ratios between 35 and 60 were loaded in three-point bending and, from the linear part of the load–deflection curve (obtained from LVDT measurements), the flexual modulus was evaluated, using a graphical method [31], to be 110 ± 1 GN m^{-2}.

4.2. Flexural and interlaminar shear strengths

4.2.1. Beams with span-to-depth ratio of 40

The "flexural" stresses at the limit of proportionality and at the peak load, for tests with 6.35 mm diameter loading rollers, were 1.40 ± 0.04 and 1.57 ± 0.08 GN m^{-2} evaluated using Equation 1. It should be pointed out that Equation 1 underestimates, with respect to Equation 11, the compressive stress by $\sim 8\%$ and overestimates, with reference to Equation 3, the tensile stress by $< 1\%$ at the limit of proportionality. Equation 1 is generally used to calculate flexural strengths of composite beams although, if non-linear deformation precedes maximum load, it overestimates, by unknown amounts, the outer fibre stresses due to bending.

Fig. 2 shows a load–displacement curve (moni-

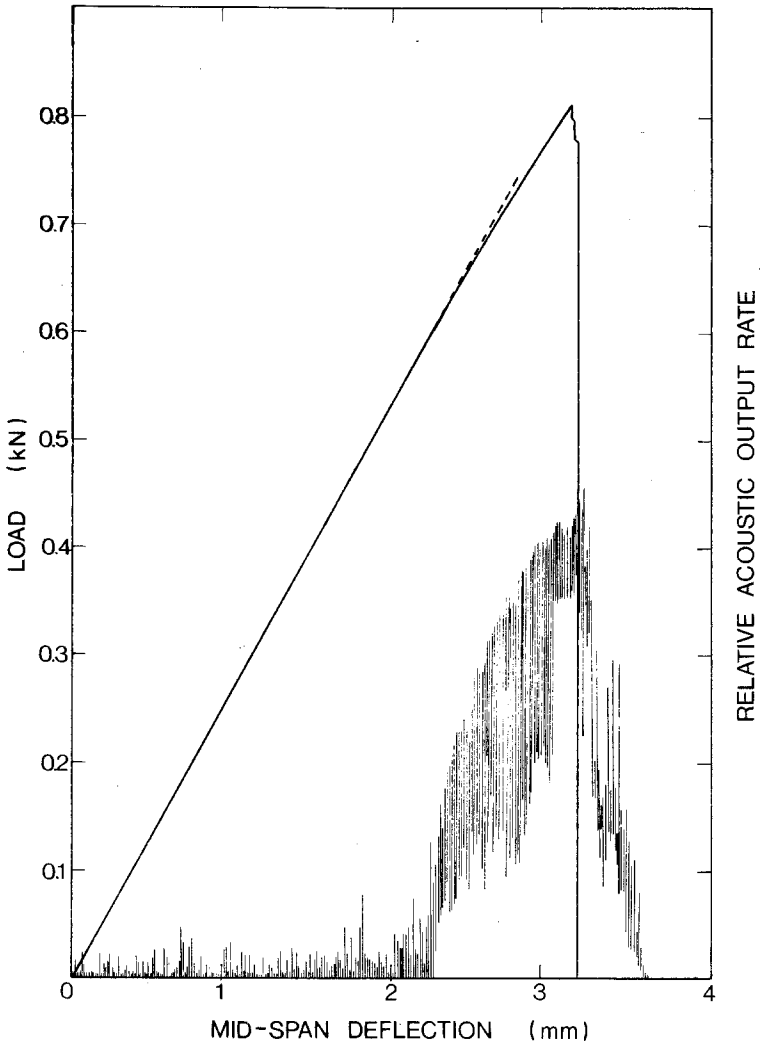

Figure 2 Typical load–deflection response of a 80 mm span CFRP specimen. Also shown is the relative acoustic emission rate measured in the range 10–100 kHz. Note that the onset of appreciable acoustic output corresponds to the departure of the deformation from Hooke's Law.

tored with a LVDT) together with the acoustic output rate. The emission was measured for the range 10–100 KHz with an attentuation of 95 dB. It is seen that an increase in output occurred at the onset of the non-linear deformation, prior to peak load. Microscopic examination of specimens whose deformation was stopped before the peak load was reached revealed local damage at the "compression" roller contact line and indications that kinking was initiated there.

Failure was catastrophic at peak loads which were attained after 4–10% non-linear deformation (measured as a proportion of peak *load*). Examination of fracture surfaces revealed compressive and tensile failure zones meeting at, approximately, the neutral axis. The compressive zones were stepped (e.g., see Fig. 3) and, at higher magnifications, it was seen that failure surfaces of individual fibres also had two zones (e.g. Fig. 3b), previously associated with tensile and compressive failure in buckling [2].

4.2.2. Beams with span-to-depth ratio of 5

4.2.2.1. Atmospheric pressure tests. Beams were tested using 6.35 mm diameter loading rollers and loads at the limit of proportionality and the peak values were noted. Using Equaiton 2, the nominal shear stresses (at the neutral axis) were $62 \pm 2\ MN\ m^{-2}$ at the limit of proportionality and $88 \pm 1\ MN\ m^{-2}$ at peak load, the so-called interlaminar shear strength. As in the long-span tests, a marked rise in the acoustic emission output took place in the non-linear region, which is now about 30% of the load-deflection curve (see Fig. 4). When a specimen was cycled between zero and progressively higher loads, irrecoverable deflection

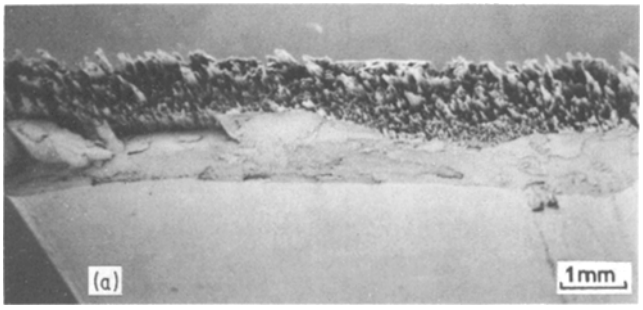

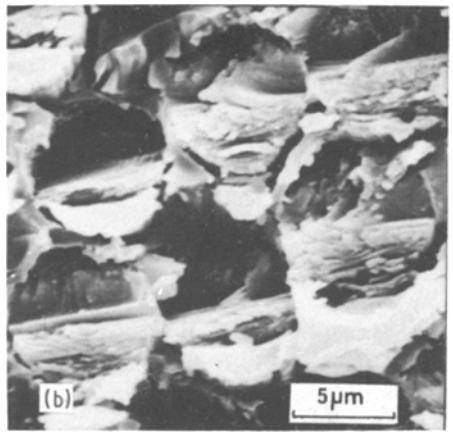

Figure 3 (a) Scanning electron fractograph of a 80 mm span CFRP specimen tested in flexure at atmospheric pressure – showing approximately equal amounts of tensile- and compressive-type failure. (b) Higher magnification of a part of the compressive region, showing demarcation of the fibre ends themselves into two regions, apparently tensile and compressive.

was detected for a load intermediate between that at the limit of proportionality and the maximum load that could be carried by the beam.

Microscopic examination of specimens unloaded at various stages on the load–deflection curve beyond the elastic limit showed the development and, once the peak load was reached, propagation of kinking from the "compression" roller. In most cases, to obtain good evidence of kink bands, it was necessary to polish through the specimen's width some way from the surface (Fig. 5). A kink band appeared to involve local buckling of the fibres in the region adjacent to the loading roller. Kink boundaries were defined by fractured fibres and formed at an inclination to the specimen surface of $\sim 30^\circ$. During the development of a kink,

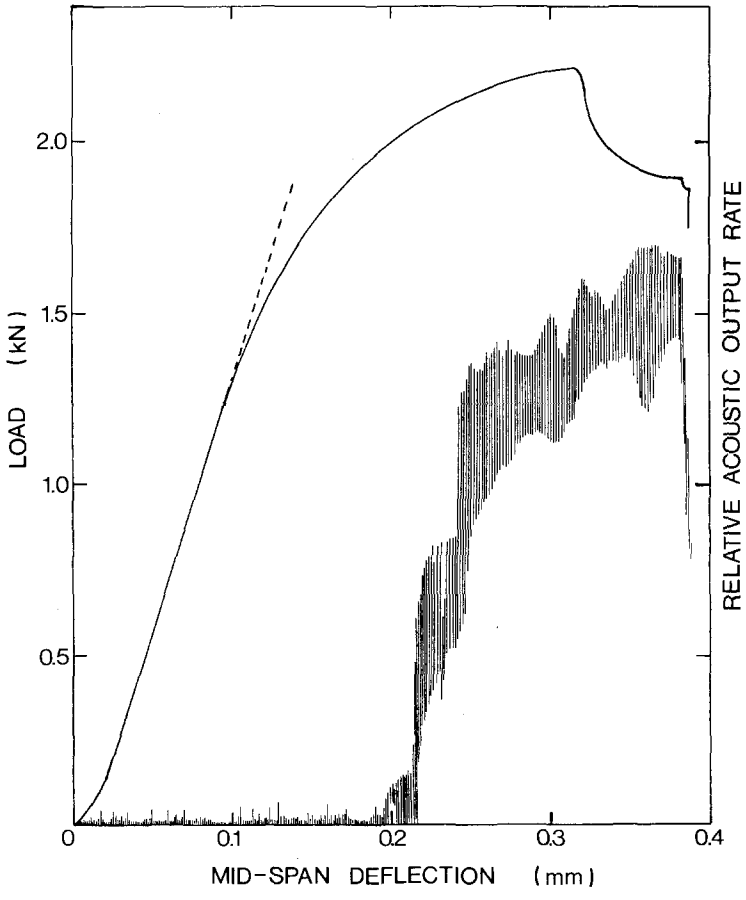

Figure 4 Typical load–deflection response of a 10 mm span CFRP specimen. Also plotted is the relative acoustic emission rate measured in the range 10–100 kHz. Note that the onset of appreciable acoustic output rate follows the departure of the load–deflection plot from linearity.

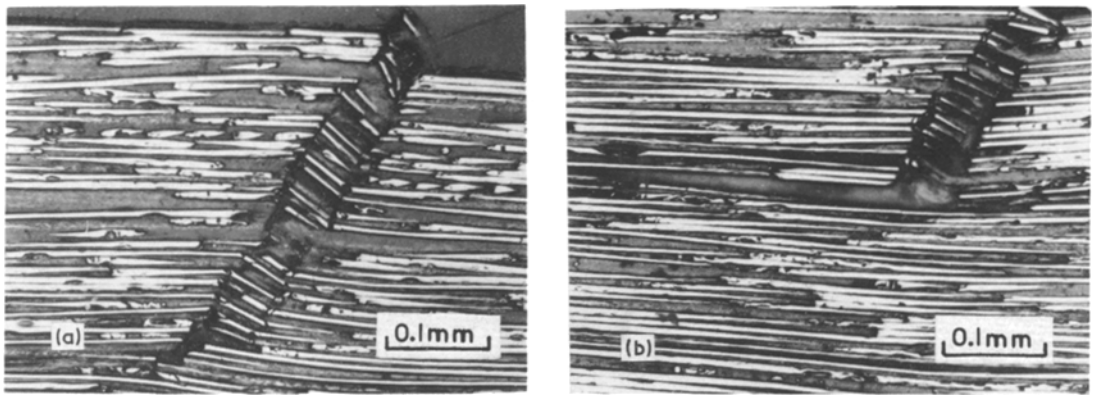

Figure 5 (a) Kink band in a sectioned 10 mm span CFRP specimen, ~ 2 mm from the original specimen surface. The specimen was unloaded shortly after the peak load was reached. (b) Interlaminar crack associated with a kink band in a similar CFRP 10 mm span specimen, which was unloaded after ~ 40% drop in load from the maximum.

fibres on either side of it were displaced laterally and the boundary appeared to rotate in the same sense as the lamellae in the band. Kink propagation, after the peak load was reached, eventually led to formation of interlaminar cracks (e.g. Fig. 5b). Delamination was not confined to the neutral plane and tended to follow interlaminar resin-rich regions (see Fig. 6). Stresses for this stage of failure could not be calculated.

4.2.2.2. Tests under superposed hydrostatic pressure. Maximum shear stresses were calculated at the limit of proportionality and the peak load according to Equation 2 and the data are presented in Fig. 7. The figure also includes the maximum tensile and compressive stresses calculated using Equations 3 and 11 and the value of the pressure. The behaviour of samples tested at pressures lower than 150 MN m^{-2} resembled that at atmospheric pressure, except that the applied load somewhat increased with pressure. At higher pressures, however, although kinking preceded failure, interlaminar cracking was suppressed. Failure surfaces had both a tensile and a compressive zone and, with increasing pressure, the boundary moved towards the compressive surface (see Fig. 8). The nominal maximum principal tensile stress at peak load was in the range 1.0–1.1 GN m^{-2} for these latter samples.

4.2.3. Beams with span-to-depth ratio of 15

This specimen configuration was chosen to test, as near as possible, flexural specimens in the hydrostatic pressure apparatus which limits the span to 25 mm. As in Section 4.2.2.2, stresses at the limit of proportionality and peak load were calculated

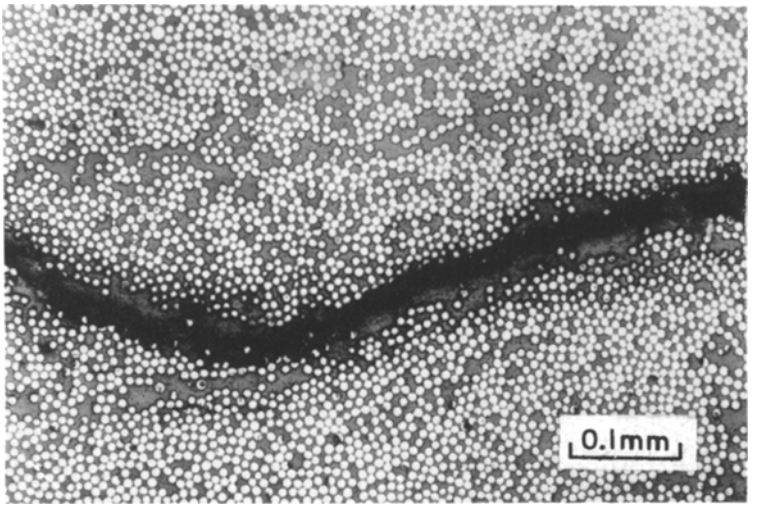

Figure 6 An "interlaminar-shear" crack photographed on the end-section of a 10 mm span CFRP beam. Its position was at about one-third depth from the concave surface and it followed resin-rich regions of the composite.

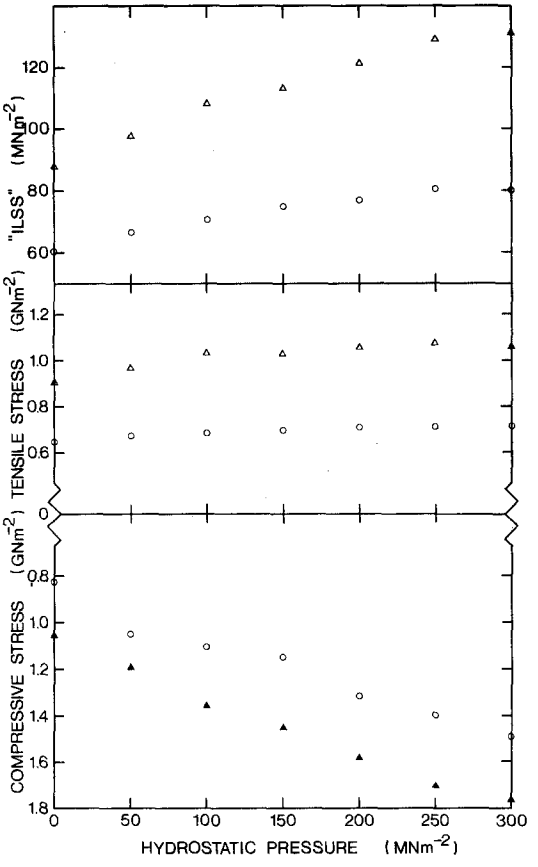

Figure 7 Maximum (interlaminar) shear, tensile and compressive stresses for 10 mm span CFRP specimens, tested under superposed hydrostatic pressure, at the limit of proportionality (○) and at peak load (△, ▲). Full symbols denote the mode of failure.

and the data are plotted in Fig. 9. At pressures up to 170 MN m^{-2} failure was initiated at the compressive faces at an approximately constant compressive stress (at the limit of proportionality) of 1.6 GN m^{-2}. Failure growth (kinking) appeared to proceed in a manner similar to that reported for the long-span atmospheric tests, except that the non-linear part of load–deflection curve was now larger, ~ 15%. Failure propagation, resulting in tensile and compressive zones meeting at about the neutral axis on the failure surfaces, also appeared to be similar (Fig. 10a).

At pressures greater than 170 MN m^{-2} failure initiation was similar, but kink propagation appeared to be suppressed, and at 300 MN m^{-2} even the compression damage seemed to have been eliminated. The apparent maximum principal tensile stress at peak loads was ~ 1.8 GN m^{-2} for the specimens tested above 170 MN m^{-2} pressure. The boundary between the tensile and com-

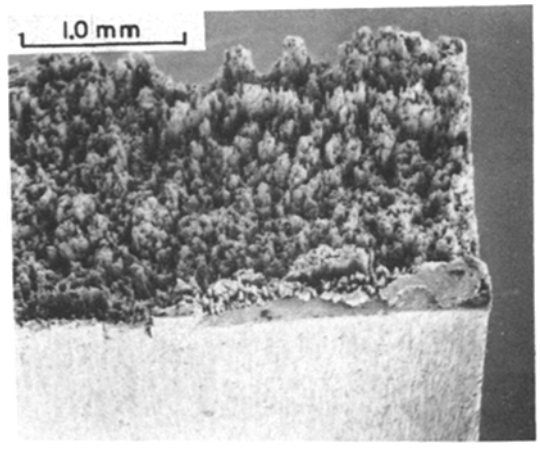

Figure 8 Scanning electron fractograph of a 10 mm span CFRP specimen tested in flexure under a superposed pressure of 300 MN m^{-2}, showing predominantly tensile-type failure, some compressive-type failure, and a total absence of interlaminar shear cracking.

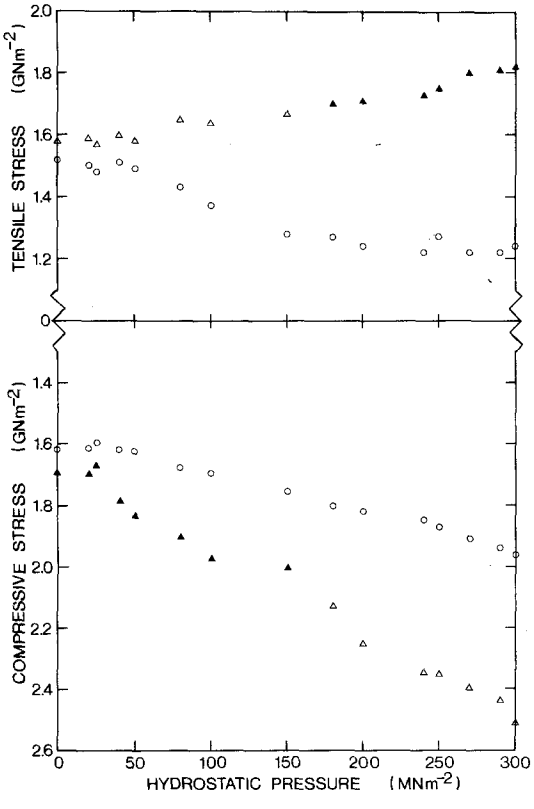

Figure 9 Maximum tensile and compressive stresses for 25 mm span CFRP specimens, tested under superposed hydrostatic pressure, at the limit of proportionality (○) and at peak load (△, ▲). Full symbols denote the mode of failure.

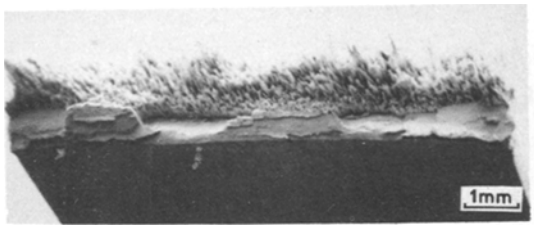

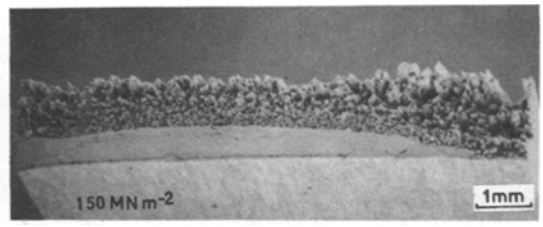

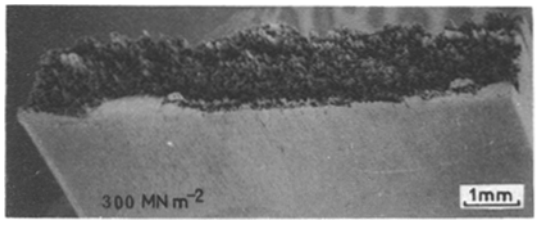

Figure 10 Scanning electron fractographs of 25 mm span CFRP specimens tested at (a) atmospheric pressure, (b) 150 MN m^{-2} and (c) 300 MN m^{-2} superposed hydrostatic pressure. Note the increase in proportion of tensile-type fracture and the reduction of fibre pull-out lengths with increasing pressure.

pressive zones on the failure surfaces moved towards the concave surface with increasing pressure (Fig. 10) and, in the tensile zone, pull-out lengths of fibres decreased with increasing pressure.

4.2.4. Four-point bend tests

Maximum tensile and compressive stresses at the limit of proportionality and peak load were calculated using the formula

$$\sigma = \frac{3Pa}{wt}, \qquad (13)$$

where P is the load, w is the width, t is the depth and a is the inner–outer roller distance (8.25 mm). Fig. 11 summarizes the strength data. Up to 125 MN m^{-2} the failures were compressive and associated with kink propagation; the apparent maximum principal compressive stress (at peak load) seemed to increase linearly with pressure. At higher pressures failure took place in the region between the loading rollers and therefore cannot be associated with local compressive damage. The apparent maximum principal tensile stress (at peak load) was ~ 1.8 GN m^{-2} for these specimens (Fig. 11). The failure surfaces had tensile and compressive regions, the latter decreasing with increasing pressure, in a similar way to the short specimens tested above 150 MN m^{-2}.

4.3. Tensile tests

The tensile strength was found to be 1.75 ± 0.03 GN m^{-2}. Tensile failure of the fibres was accompanied by longitudinal splitting.

5. Discussion

The importance of *local* stresses is recognized in analyses of bending of even isotropic materials [22–25]; it does not appear to have received sufficient attention, however, in the consideration of failure mechanisms of fibre-reinforced plastics. Although our experiments were carried out with pultruded material incorporating type III surface-treated carbon fibres, the data may have a wider relevance. Evidence from experiments described in this paper indicates that behaviour in flexure that

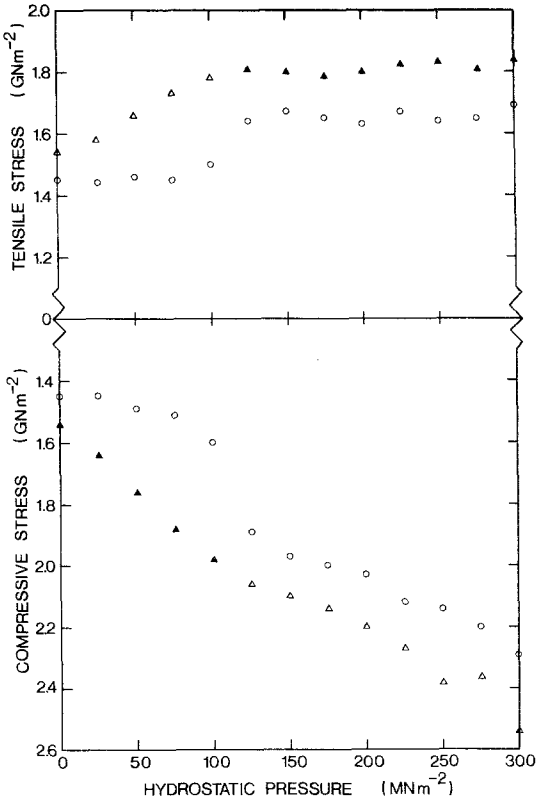

Figure 11 Maximum tensile and compressive stresses for CFRP four-point bend specimens, tested under superposed hydrostatic pressure, at the limit of proportionality (○) and at peak load (△, ▲). Full symbols denote the mode of failure.

does not obey Hooke's Law can be associated with local damage. At the "compressive" loading rollers the stress systems include, in addition to the longitudinal compressive stress due to bending modified by Hertzian stresses (Equation 11), transverse compressive stresses. Parallel to the specimen thickness compressive, Hertzian stresses result directly from roller contact (Equation 12) and across the specimen width the roller restrains the development of anticlastic curvature. The damage caused by this triaxial compression led to the initiation of kinking, which has also been described as local compressive buckling [3] or compression creasing [5].

It is important to note that this failure initiation stage is accompanied by some relief of the local stresses and that failure growth by this mode requires higher loads. This rise may be of such magnitude that, before a critical condition for failure propagation is reached, by the continuation of this process, the criterion for another mechanism of failure is satisfied (i.e. tensile failure). It seems that the initiation stage of the tensile failure process is the most difficult but, in principle, the *initiation, growth* and *propagation* stages of the tensile process should be considered as well as those of the compressive process. In our studies of pultruded CFRP beams there was no evidence of interlaminar shear-initiated failure, although the final rupture process at atmospheric pressure, as the load-carrying capacity of small-span beams decreased with increasing deflection, was through interlaminar delamination.

In general, with increasing strain and decreasing load, the same (compressive or interlaminar) failure modes may propagate or, if compressive failure is inhibited (e.g. by superposed pressure), the tensile mode may operate on "beams" of decreasing depth. This is the interpretation suggested for the displacement, with increasing pressure, of the tensile–compressive failure mode boundary towards the *concave* face, which *reduces* the maximum principal tensile stress.

The relevant mechanisms to be considered in the failure of pultruded CFRP in flexure are thus:

(a) initiation of kinking (by "compression" roller or rollers);

(b) propagation of kinking towards the tensile surface;

(c) kink-initiated delamination;

(d) tensile failure (initiated by fibre fractures) propagating towards the compressive surface.

Acoustic emission and load cycling data, as well as microstructural observations, indicated that, at atmospheric pressure, local compression damage was initiated at about 70% of the peak load for short-span specimens, about 95% for three-point and about 90% for four-point flexural specimens, respectively. The resultant redistribution of stresses and non-linear load–deflection curves implies that, generally, the conventional elastic beam formulae cannot be used. Regarding the maximum tensile stress, on the undamaged convex beam surface, σ_T from Equation 1 is an overestimate if the beam retains its integrity.

For the flexural specimens with span-to-depth ratio of 40, however, the error associated with Equation 1 is small, yet the conventionally calculated strength ($\sim 1.54\,GN\,m^{-2}$) was less than the value determined in direct tensile testing ($\sim 1.75\,GN\,m^{-2}$). If the two parameters referred to the *same* property and Weibull-type analysis [32] were relevant, flexural strength should have been higher than the tensile strength. A tensile-initiated failure process was in fact observed when the span-to-depth ratio was 80, but at a ratio of 40 there was evidence of kink initiation before the peak load was reached. This appeared to be associated with kink growth and, as concurrently higher tensile stresses resulted from load redistribution, fibre fracture took place on the convex surface. Thus the tensile-failure mode propagated towards the compressive surface, as compressive failure involving microbuckling propagated from the kink in the opposite direction. Zones of the two failure modes met at, approximately, the neutral surface in atmospheric pressure tests (see Fig. 3).

For the three-point bend specimens with span-to-depth ratio of ~ 15 and the four-point bend specimens these flexural strength values were similarly 1.54 and $\sim 1.56\,GN\,m^{-2}$, respectively. The failure mode differed in that kinking was more extensive and tensile failure more difficult to initiate; tests could be easily stopped with no sign of tensile damage but with compression damage extending several hundred micrometers. This was favoured in three-point bend specimens by the smaller span and depth of the beams and smaller diameter of the loading rollers and appeared to start at smaller fractions of the peak load, which is associated with kink propagation. The results of experiments carried out under superposed hydrostatic pressure support this interpretation.

In general the application of pressure, $-H$, leaves the shear stresses unaffected but decreases

the tensile stresses and increases the compressive stresses by $|H|$. It is these maximum and minimum principal stresses which are plotted in Figs 7, 9 and 11. It is to be noted that, whereas the compressive stress for initiation of damage remained relatively unaffected by pressure for both types of specimen, the apparent stress at peak load for the compressive failures varied with pressure.

In CFRP, kink-controlled failure has previously been shown to become more difficult [5] with increasing pressure. It appears that pressures of 120 and nearly 300 MN m^{-2} for the four- and three-point bend specimens, respectively, were sufficient to suppress this failure mode. Above these respective transition pressures the peak loads corresponded to a nearly constant and, it is suggested, a critical tensile stress of $\sim$ 1.8 GN m^{-2}, approximately equal to the axial tensile strength ($\sim$ 1.75 GN m^{-2}). Because of the preceding damage the flexural values may well be underestimates and it is possible that the effect of pressure, which has been shown to strengthen the resin and reduce fibre pull-out lengths [17], was to increase the composite tensile strength. Failure of all these specimens was progressive and it is suggested that, as kinking became more difficult at higher pressures, the compressive failure mode was suppressed and tensile failure proceeded by breaking, effectively, beams of continuously decreasing depth. Accordingly the tensile zone of the failure surface increased with increasing pressure. It should be pointed out that no evidence of individual fibre failure by shear was found, although the maximum shear stresses for type III carbon-fibre composite (up to 1.1 GN m^{-2}) exceeded those reported by Ewins and Ham for type I and II carbon-fibre composites ($\sim$ 0.9 GN m^{-2}) [2].

The so-called interlaminar shear failure mode was initiated in all atmospheric pressure tests by kinking. The clear association of the stresses at both the end of linear deformation and the peak load with local conditions at the "compressive" roller, as exemplified by changing the roller diameter [4] or incorporating steel wires on the compressive face of the short-span specimen [13], was further supported by acoustic emission and microscopic studies. Acoustic emission significantly increased in the non-linear range (Fig. 4) and damage was detected when specimens were unloaded before the peak load was reached. It is suggested that (as also for longer span specimens) kink initiation, involving microbuckling of fibres, and shear of the matrix should be associated with the onset of non-linear deformation. This matrix flow was followed by further buckling of the fibres, resulting in the formation of a kink at loads near the maximum. Kink initiation, growth and propagation (probably at peak load) were a function of the local as well as the general stresses, hence the influence on ILSS of roller diameter [14] or plastically deforming steel wires inhibiting kinking [13].

Delamination on the other hand was not initiated until a relatively late stage in this progressive failure process, at deflections beyond that at the peak load which is conventionally used to calculate ILSS. No physical significance should therefore be attached to this parameter calculated assuming linear deformation. It is interesting to note that the values of ILSS generally quoted, 80–100 MN m^{-2}, are approximately twice the shear strength of the matrix. Propagation of the delamination (interlaminar cracking) may be governed by an energy criterion, as postulated by Kendall [33].

Results of tests under pressure support our model of failure. Kinking under pressure requires higher compressive stresses and accordingly the apparent ILSS (which, if primarily a resin shear property, should increase weakly with increasing pressure [34]) was found to increase markedly from $\sim$ 90 to $\sim$ 120 MN m^{-2} at $\sim$ 150 MN m^{-2} pressure (Fig. 7) when interlaminar failure was suppressed. At higher pressures the apparent tensile stresses at failure were appreciably lower (1.0–1.1 GN m^{-2}) than the composite tensile strength. This discrepancy is attributed primarily to the redistribution of stresses during non-linear deformation (rising to 38% at 300 MN m^{-2} pressure) when kinks were formed and grew by fibre failure. The beam depth in such situations was effectively reduced and accordingly the tensile stress on the undamaged convex surface was appreciably higher than that calculated using Equations 1 or 3 before tensile failure was initiated. Its propagation was accompanied by kink propagation in the opposite sense and not delamination.

It is concluded that the beam test, particularly three-point bending of specimens with span-to-depth ratio less than 40, is inadequate for evaluating actual composite properties. At atmospheric pressure with conventional specimen sizes, spans and rollers, failure initiation and frequently the

actual failure process result from the local damage (kinking) caused by "compressive" roller or rollers. Unfortunately it was not possible to derive a critical stress criterion for the initiation of this process [29]. The maximum loads recorded, and therefore the apparent flexural or interlaminar shear strengths, were associated with kink propagation. Bending, however, particularly under complex loading, is the principal mode of deformation of useful composite components. The work described demonstrates the importance of local damage (kink initiation) and its role in the redistribution of stresses, kink growth (probably necessitating higher general stresses) and failure propagation at general stresses frequently lower than those required for kink growth. This can lead to an apparent size effect on strength; thus, if local stresses were neglected, the flexural (tensile) strength of short-span specimens was calculated (under superposed hydrostatic pressure) to be $\sim 1.0\,\mathrm{GN\,m^{-2}}$, whereas in direct tensile testing the value obtained was $\sim 1.75\,\mathrm{GN\,m^{-2}}$. It is accordingly suggested that these data have some bearing on design of composite components as well as testing of composite beam specimens.

Acknowledgements

The authors gratefully acknowledge discussions of the concentrated loading problems with Dr T. H. C. Childs of the University of Bradford, who also derived Equations 11 and 12 of this paper. The work described formed part of a CASE programme supported by British Rail and the Science Research Council, who provided a research studentship for one of us (TVP). Thanks are due for the provision of laboratory facilities at Bradford to Professor D. Bijl and at the British Rail Technical Centre, Derby, to Mr A. W. Denham.

References

1. J. V. MULLINS, J. M. BERRY and A. GATTI, *J. Comp. Mats.* 2 (1968) 82.
2. P. D. EWINS and A. C. HAM, Royal Aircraft Establishment Technical Report Number 73057, August, 1973.
3. B. W. ROSEN, Mechanics of Composite Strengthening, American Society of Metals Seminar, Philadelphia, Pa, October, 1964.
4. J. E. BAILEY, M. G. BADER and M. JOHNSON, Conference on Designing to Avoid Mechanical Failures, Cranfield Institute of Technology, January 1973 (Plastics Institute, London, 1973).
5. C. R. WEAVER and J. G. WILLIAMS, *J. Mater. Sci.* 10 (1975) 1323.
6. C. R. CHAPLIN, *J. Mater. Sci.* 12 (1977) 347.
7. A. G. EVANS and W. F. ADLER, *Acta Metall.* 26 (1978) 725.
8. J. M. DINWOODIE, *Wood Sci. Technol.* 8 (1974) 56.
9. M. S. PATERSON and L. E. WEISS, *Geol. Soc. Amer. Bull.* 77 (1966) 343.
10. L. E. WEISS, Proceedings of the Conference on Research on Tectonics, Ottawa, 1968, edited by A. J. Baer and D. K. Norris (Geological Survey of Canada, 1969), p. 294.
11. Grafil, Test Methods, Courtaulds, Coventry, 1975.
12. M. FUWA, A. R. BUNSELL and B. HARRIS, *J. Mater. Sci.* 10 (1975) 2062.
13. P. D. BRADLEY and S. J. HARRIS, *J. Mater. Sci.* 12 (1977) 2410.
14. T. V. PARRY and A. S. WRONSKI, in "High Pressure Science and Technology" edited by B. Vodar and Ph. Marteau (Pergamon Press, Oxford, 1980) p. 299.
15. J. W. HITCHON, W. H. McCAUSLAND and D. C. PHILLIPS, AERE Report No. R8217, November 1975.
16. A. S. WRONSKI and R. J. HOWARD, in "High Pressure Science and Technology" edited by B. Vodar and Ph. Marteau (Pergamon Press, Oxford, 1980) p. 296.
17. J. J. DIBB, Ph.D. thesis, University of Bradford, 1975.
18. T. A. COLLINGS, *Composites* 5 (1974) 108.
19. S. P. TIMOSHENKO, "Strength of Materials" 3rd edn. (Van Nostrand, New York, 1969) p. 92.
20. C. WILSON, *Phil. Mag.* 32 (1891) 481.
21. M. M. FROCHT, "Photoelasticity" Vol. II, (John Wiley and Sons, New York, 1948) p. 104.
22. E. A. ALMOND and B. ROEBUCK, *Metal Sci.* 11 (1977) 458.
23. A. S. WRONSKI, L. B. HUSSAIN-AL-YASIRI and F. L. JAGGER, *Powder Metall.* 22, (1979) 109.
24. T. von KARMAN and F. SEEWALD, *Abhandl. Aerodynam. Inst. Tech. Hochschule* 7 (1927) 3.
25. S. P. TIMOSHENKO and J. N. GOODIER, "Theory of Elasticity" 3rd edn. (McGraw Hill, New York, 1970) p. 113.
26. M. T. HUBER and S. FUCHS, *Phys. Zeit.* 15 (1914) 298.
27. H. PORITSKY, *Trans. ASME, J. Appl. Mech.* 17 (1950) 191.
28. T. H. C. CHILDS, private communication, 1980.
29. T. V. PARRY, Ph.D. thesis, University of Bradford, 1980.
30. M. S. STUCKE and A. S. WRONSKI, *Proc. Brit. Ceram. Soc.* 25 (1975) 109.
31. H. WELLS and N. L. HANCOX, *Composites,* 2 (1971) 147.
32. W. WEIBULL, *Ing. Vetenskaps. Akademiens Hadlingar (Stockholm)* 151 (1939) 1.
33. K. KENDALL, *J. Mater. Sci.* 11 (1976) 638.
34. A. S. WRONSKI and M. PICK, *J. Mater. Sci.* 12 (1977) 28.

Received 29 May and accepted 10 July 1980.